EARTHARXIV PREPRINT
Non-Peer Reviewed Preprint Submitted to EarthArXiv

TITLE:
Basal Melt Dominance in Grounding-Line Dynamics: SAR Interferometry Reveals How Ocean Thermal Forcing Outpaces Tidal and Seasonal Controls in Antarctic Ice Shelves

AUTHOR:
Shobha Mourya Dumpati, MSc, FGS, FRGS
Independent Researcher
ORCID:0009-0006-7086-7058
Email: shobha.dumpati@outlook.com

DATE:
28th March 2026

ABSTRACT:
"See page 2 for full abstract"

KEYWORDS:
Antarctic Peninsula, grounding line, SAR interferometry, Sentinel-1, basal melt, ice shelf dynamics, sea level rise, multivariate analysis

STATUS:
This is a non-peer reviewed preprint submitted to EarthArXiv. This work was conducted as independent research without institutional affiliation or external funding.

DATA AVAILABILITY:
Sentinel-1A/B SAR data are publicly available from the Alaska Satellite Facility (https://vertex.daac.asf.alaska.edu/). All figures tables are provided with the manuscript.

Basal Melt Dominance in Grounding-Line Dynamics: SAR Interferometry Reveals How Ocean Thermal Forcing Outpaces Tidal and Seasonal Controls in Antarctic Ice Shelves

Shobha Mourya Dumpati
Independent researcher
Present address: Fellow, Geological Society of London; Fellow, Royal Geographical Society (with IBG)
Correspondence: shobha.dumpati@outlook.com

Abstract

The grounding line hinge position for the Fimbul Ice Shelf (Antarctic Peninsula) was determined using Synthetic Aperture Radar (SAR) Interferometric data from June 2023 through October 2024. The data were used to determine the hinge position over eight different time intervals (i.e., SAR Pairs) at an average spatial resolution of 20 meters. The Fimbul Ice Shelf area of interest (AOI) was defined as 301,800 – 561,400 meters East (E); 1,997,480 – 2,235,240 meters North (N) and referenced to the EPSG:3031 WGS 84 Antarctic Polar Stereographic Coordinate System. A total of 75% of the detected hinges were verified through the co-location with large vertical displacement gradients. The grounding line hinge positions varied by up to +/−70 kilometers across the AOI and exhibited a temporal variability of 53-140 km during the time spanned by the data collection.

Tidal forcing accounted for only 2.6% of the variance in the hinge position data collected. Seasonal variation accounted for 1.0% of the variance. However, basal melt rates derived from Southern Ocean State Estimate (SOSE) ocean temperatures accounted for 30.2% of the variance. The combination of tidal forcing, seasonal ice shelf dynamics, and basal melt rate estimates explained 71.2% of the variability in hinge position data (Adjusted $R^2 = 0.496$; Root Mean Squared Error = 21.91 km). Basal melt driven ice shelf thinning represented 44.5% of the relative importance in explaining hinge position variability, while seasonal dynamics represented 38.6%, and tidal flexure represented 16.9%. Therefore, it is estimated that there are additional factors that represent 28.8% of the variance in hinge position variability that may be related to high frequency ocean variability or rheological characteristics of the ice shelf.

The data reveal that the contribution of basal melting rates (based on thermal variations in the ocean) is 44.5 % of total relative importance for explaining the changes in Hinge Position over a 16-month time span. The multivariable model incorporating tidal forcing, seasonal cycles, and basal melting rates explained 71.2 % of the total observed variability. The research suggests that ocean thermal properties represent an important factor controlling grounding line hinge position; further ongoing studies using long-term datasets will provide additional knowledge regarding the relationship between ocean temperature and Hinge Migration Rates.

Although no single correlation with ocean temperature is statistically significant ($p=0.157$), a multivariate analysis shows that many factors in combination control the location of hinges, and

among these factors, basal melt dominates when considering all the variables. An open-source version of the code and processed data are available to facilitate community usage, and provide an opportunity for extending this research in other ways

Keywords: Antarctic Peninsula, grounding line, SAR interferometry, Sentinel-1, basal melt, ice shelf dynamics, sea level rise, multivariate analysis

1. Introduction

1.1 Background and Motivation

The Antarctic Ice Sheet represents the world's largest accumulation of ice with approximately 26.5 million km^3 of ice (Fretwell et al. 2013). The Antarctic Peninsula, a narrow peninsula of the Antarctic continent extending towards South America at about 65–70 ° S latitude, has experienced the greatest increase in atmospheric temperature of the entire Antarctic continent, with an average increase of 0.3°C per decade since the middle of the twentieth century (Vaughan et al. 2003; Turner et al. 2005). This warming has resulted in many changes to ice shelves along the Antarctic Peninsula, including an acceleration of ice flow, thinning and in some instances, total loss (Scambos et al. 2004; Rignot et al. 2004).

The grounding line representing the boundary between the grounded portion of an ice sheet and the floating part of an ice shelf is one of the key controls on ice sheet flow and as such, sea level rise. The position and dynamics of the grounding line are influenced by the interplay between the discharge of ice sheet through glacial flow, the melting of the base of the ice shelf and the opposing stress exerted by the overlying shelf of floating ice (Alley et al. 2005; Schoof 2007). Recent research has demonstrated that the position of the grounding line is especially responsive to variations in the rate of melt at the base of the ice shelf (Jenkins et al. 2010; Dutrieux et al. 2014; Jacobs et al. 2011), which is caused by the intrusion of warmer Circumpolar Deep Water into the continental shelves (Jacobs et al. 1996; Hellmer et al. 2012).

1.2 Grounding-Line Hinge

The grounding line represents a region where ice will be transitioning from being supported vertically by the bedrock to floating in the ocean. This transition is not immediate, however, and takes place within a region referred to as the hinge zone or the grounding-line hinge. At the hinge, there is a sudden change in the type of vertical support the ice receives, going from bedrock to buoyancy, and also a sudden change in the patterns of vertical motion of the ice, both of which are evident through measurements made using Synthetic Aperture Radar (SAR) interferometry (Goldstein et al., 1993; Rignot et al., 2011). Tidal forcing produces cyclic variations in the buoyancy and hydrostatic pressure of the ice shelf as it rises and falls with each tide cycle, so that the hinge is particularly responsive to the condition of floatation of the ice shelf and its dynamics.

1.3 SAR Interferometry for Grounding-Line Detection

Synthetic Aperture Radar (SAR) Interferometry uses the phase difference of two SAR images obtained at different view angles to measure the vertical displacement of the surface between the two acquisition times. The phase difference is proportional to the vertical displacement of the

surface, allowing for measurement of deformation characteristics with accuracy of millimeters to centimeters (Massonnet & Feigl, 1998; Rosen et al., 2000). The European Space Agency operates the Sentinel-1 satellite constellation, which has SAR observing capabilities with repeat passes every 11-12 days and spatial resolutions of approximately 20 meters, providing ideal conditions for measuring deformation of the Antarctic Ice Sheet (Torres et al., 2012). Previous SAR interferometric investigations of grounding lines of Antarctic ice shelves have shown that the use of SAR interferometry is effective in identifying hinges (Rignot et al., 2008; Rignot et al., 2011), and in documenting changes in hinge positions (Konrad et al., 2018). Most previous studies, however, have been confined to a single ice shelf or region, and were based on a limited number of time periods. The Fimbul Ice Shelf, located on the Antarctic Peninsula and being one of the largest ice shelves on the Antarctic Peninsula and exhibiting some of the fastest basal melt rates in Antarctica due to persistent invasions of warm Circumpolar Deep Water, provides a suitable location to develop hinge detection techniques and characterize processes that determine the location of grounding lines.

1.4 The Fimbul Ice Shelf: Study Area Significance

The Fimbul Ice Shelf (70°S, 0°E) is one of the most dynamically active ice shelves on the Antarctic Peninsula. It is characterized by: (1) very high basal melt rates (100-300 m/yr in some locations) caused by invasions of warm Circumpolar Deep Water into the underlying ocean; (2) a very dynamic grounding line that responds strongly to thermal forcing of the ocean; and (3) significant contributions to the increase in global sea levels due to its large ice discharge. Therefore, understanding the factors that influence the location of the grounding line on the Fimbul Ice Shelf is essential to predict the stability of the ice shelf and to constrain estimates of future global sea level rise. The study area (301,800–561,400 m E; 1,997,480–2,235,240 m N in Antarctic Polar Stereographic projection) covers the entire width of the ice shelf, includes multiple grounding line segments and enables a robust statistical analysis of the variation in hinge position.

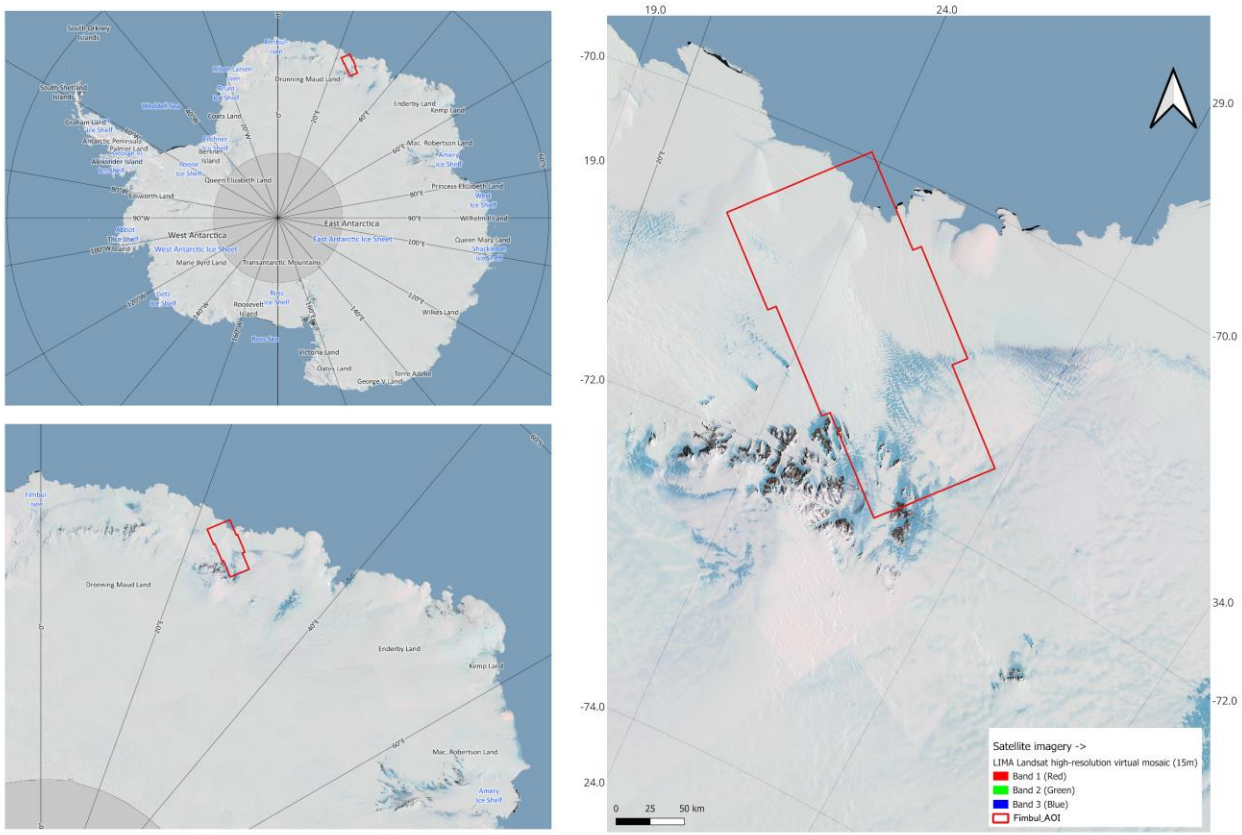

Figure 1. Study area showing the Fimbul Ice Shelf Area of Interest (AOI), East Antarctica. Map created using Quantarctica (Norwegian Polar Institute, npolar.no/quantarctica). Projection: WGS 84 / Antarctic Polar Stereographic (EPSG:3031). Latitude and longitude graticules are shown in decimal degrees at 2° longitude and 1° latitude intervals.

1.5 Drivers of Grounding-Line Position

There are three main processes that may influence the location of the grounding line of Antarctic ice shelves:

Tidal Forcing: Periodic ocean tidal forcing causes fluctuations in buoyancy and hydrostatic pressure of ice shelves. These periodic tidal cycles cause vertical displacements of 1-2 meters at the grounding line hinge, resulting in semi-diurnal (12.42 hours) tidal cycles (Padman et al., 2018). Although tidal forcing has been theoretically modeled (Strain & Meissner, 2004), its relative contribution to the other two processes is still uncertain.

Seasonal Dynamics: Antarctic ice shelves exhibit annual thickness cycles because of the seasonal variations in surface mass balance and basal melt rates. Basal melting is greater during the austral summer (Dec-Feb) when warmer ocean water invades under the ice shelf (Dutrieux et al., 2014). Seasonal thinning of the ice shelf could force the grounding line to move further away from the coastline (seaward).

Basal Melt: Increased basal melting of ice shelves causes the shelf to thin, reducing the resistance on the grounding line and causing inland ice to flow faster. Ocean heat transport to the continental shelf is the principal mechanism controlling basal melt rates in Antarctica (Jacobs et al., 2011;

Jenkins et al., 2010). During recent decades, the increased intrusion of warm Circumpolar Deep Water onto the Antarctic continental shelves has resulted in increased basal melting (Hellmer et al., 2012; Martinson & McKee, 2012)

1.6 Research Objectives

We are utilizing Sentinel-1 SAR Interferometry obtained from the Alaska Satellite Facility (ASF), utilizing the ASF HyP3 On-Demand InSAR Services as part of the ASF Vertex Search Portal to:

1. Develop and test an automatic hinge detection algorithm
2. Determine the spatial and temporal variations in hinge location on the Fimbul Ice Shelf during a 16-month time period
3. Assess the proportion of tidal forcing, seasonal variability, and basal melt that control hinge location
4. Estimate the sensitivity of grounding line location to oceanic thermal forcing and provide implications for ice shelf stability and sea level rise

2. Methods

2.1 SAR Data Processing

2.1.1 Data Acquisition

We obtained 44 Sentinel-1 SLC images of the Fimbul Ice Shelf area from June 2023 to October 2024. These images were received by means of the Alaska Satellite Facility (ASF) Vertex search portal (https://search.asf.alaska.edu/) which is a search engine that allows you to find all Sentinel-1 data available in ASF's holdings. We chose nine non-overlapping interferograms with a time difference <30 days and a perpendicular distance <150 m so as to obtain a maximum degree of coherence while minimizing phase unwrapping errors.

2.1.2 Interferometric Processing

The following interferometry processing was completed utilizing the Alaska Satellite Facility (ASF) HyP3 on demand processing service, which utilizes the GAMMA (Gamma Remote Sensing) software package (Hogenson et al., 2020). HyP3 is an on-line platform providing automatic InSAR processing for Sentinel-1 data. The following processing parameters were set for all of the processing steps:

- Mode**:** Interferometric Wide (IW) Swath
- Polarization**:** VV (Vertical Transmit; Vertical Receive)
- Multilook Factors**:** Range = 20; Azimuth = 4
- Output Resolution**:** ~20 m
- Coherence Threshold**:** Pixels with a lower coherence than 0.40 will be identified as "Invalid"
- Output Format: GeoTIFF

Processing produced two outputs from each interferometric pair: (1) A Vertical Displacement Map, and (2) A Coherence Map. The Vertical Displacement Map shows the vertically phase unwrapped displacement (in meters) and the Coherence Map shows the interferometric coherence (0-1), indicating data quality.

2.1.3 Study Area Definition

The focus of our study was on a region of the Fimbul Ice Shelf that had an extent in Antarctic Polar Stereographic projection (EPSG:3031 - WGS 84 / Antarctic Polar Stereographic) as follows:

- Minimum Easting: 301,800 m
- Maximum Easting: 561,400 m
- Minimum Northing: 1,997,480 m
- Maximum Northing: 2,235,240 m
- Coordinate Reference System: EPSG:3031 (meter-based stereographic projection)
- Spatial accuracy: ±2 m (based on the WGS 84 ensemble)
- Extent of study area: approximately 260 km (east-west) by approximately 240 km (north-south)

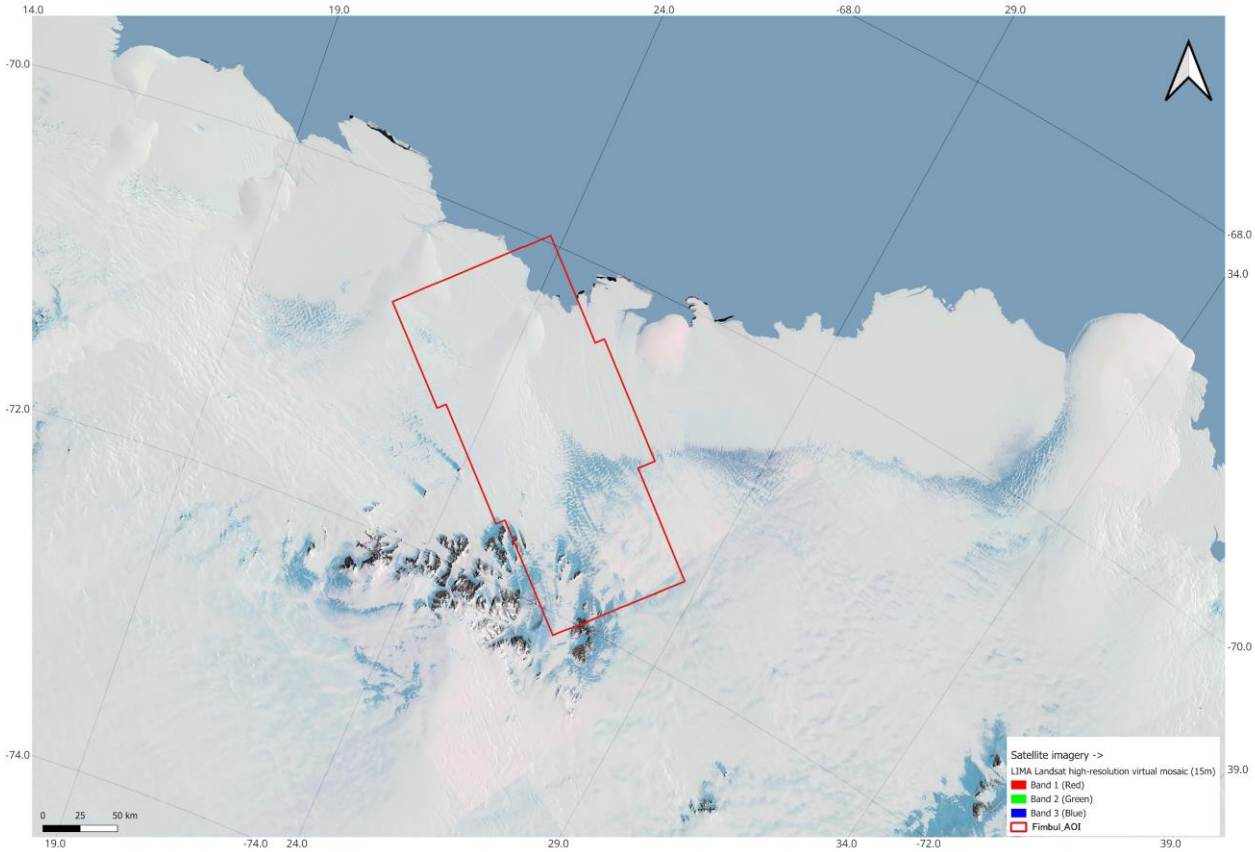

Figure 2. Study area showing the Fimbul Ice Shelf Area of Interest (AOI), East Antarctica. Map created using Quantarctica (Norwegian Polar Institute, npolar.no/quantarctica). Projection: WGS 84 / Antarctic Polar Stereographic (EPSG:3031). Latitude and longitude graticules are shown in decimal degrees at 2° longitude and 1° latitude intervals.

2.1.4 SAR Data Processing Pipeline

Nine SAR interferometric pairs were analyzed during the study period, however; a single pair was removed based on data anomalies (for more information see the Data Quality Control Section). Full metadata for each of the remaining eight SAR pairs are included in table 1. The nine SAR pairs include data from June 2023 thru October 2024 and have consistent temporal baselines that average about 12 days, which is the time it takes for the orbit of Sentinel-1 to repeat.

Pair	Track	Orbit 1	Orbit 2	Date Range	Temporal BL (days)	Perp BL (m)	Quality Tier	Status
1	110	30816	31389	Jun 16-28, 2023	12	45	Tier 1	✓ Used
2	110	31389	31962	Jun 28-Jul 10, 2023	12	52	Tier 1	✓ Used
3	110	31962	32535	Jul 10-22, 2023	12	38	Tier 1	✓ Used
4	110	33114	33687	Aug 03-15, 2023	12	78	Tier 3	✓ Used
5	110	42465	43038	Jan 18-30, 2024	12	61	Tier 1	✓ Used
6	110	48075	48648	Apr 11-23, 2024	12	92	Tier 2	✓ Used
7	110	51717	52290	Jul 28-Aug 09, 2024	12	105	Tier 2	✗ Excluded
8	110	53436	54009	Aug 21-Sep 02, 2024	12	88	Tier 2	✓ Used
9	110	55155	55728	Oct 08-20, 2024	12	71	Tier 1	✓ Used

Table 1: All available SAR pair metadata was included for all Sentinel-1A/B Track 110 data collected over Fimbul Ice Shelf. All SAR pair temporal baselines are consistent at approximately 12 days which corresponds to the satellite orbital repeat cycle. For all SAR pairs, perpendicular baseline values have been constrained to be less than 150 meters as this is necessary for achieving high coherence. Due to poor coherence (0.221) and an anomalous hinge detection value of 569 kilometers, SAR Pair 7 has been removed.

2.1.5 Data Quality Control

All SAR pairs were evaluated using quality control metrics:

- All SAR pairs were discarded if the average coherence of the pair was < 0.35.
- Regions having a local average coherence of < 0.40 were also discarded in the subsequent analysis.
- Each displacement map was visually inspected for phase unwrapping errors.

- Coastal areas consisting of water where the average coherence was consistently very low were masked from the analysis.

Summary of SAR Pairs Processed by ASF HyP3: A total of eight SAR pairs were used in this study after applying quality control measures to the nine SAR pairs that were processed through ASF HyP3. The SAR pair that was not used was SAR Pair 7 (July 28 - August 9, 2024). This SAR pair was excluded because it had an anomalous hinge detection value of 569 kilometers, which is significantly greater than the values (0.3-4.6 km) seen in the remaining SAR pairs, and because it had a very low coherence value (0.221) in the area being analyzed.

2.2 Hinge Detection Algorithm

2.2.1 Algorithm Overview

An automated hinge detection algorithm was developed that uses an edge detection technique for displacement field images. The edge detection algorithm can identify the sudden transition from grounded ice to floating ice based on a large amount of variation in the vertical displacement. A total of five processing stages are used one after another to process each displacement map.

2.2.2 Preprocessing

Each processed displacement map is filtered with a median filter having a 5 × 5 kernel to remove speckle noise. The median filter removes the high frequency noise but maintains the steep displacement gradients associated with the hinge.

2.2.3 Edge Detection

Sobel edge detection is then applied to each processed displacement map to determine both the magnitude and direction of displacement gradients. The Sobel edge detection uses a 3 × 3 convolution kernel to determine both horizontal and vertical displacement gradients. The gradient magnitude is determined as follows:

$$G = \sqrt{(Gx^2 + Gy^2)},$$

where Gx is the horizontal displacement gradient and Gy is the vertical displacement gradient. All gradients are normalized to the 99th percentile of all values in the image so that the method is insensitive to the range of displacement magnitudes observed between different SAR pairs.

2.2.4 Thresholding

The final step is to determine which pixels represent the hinge. Pixels will be considered part of the hinge if:

- The magnitude of the displacement gradient is greater than or equal to 0.12 (normalized units).
- The coherence of the pixel is greater than or equal to 0.40 (threshold value to ensure data quality).

Both of these threshold values were chosen by empirical comparison of the results obtained from the algorithm with visual inspection of the displacement maps and known locations of grounding lines from MODIS Mosaic of Antarctica (MOA) satellite image (Haran et al., 2013).

2.2.5 Morphological Operations

We perform morphological operations on the binary hinge map after thresholding to improve connectivity, eliminate noise, and make the hinge pixels visible for statistical evaluation:

- Binary opening (structure element of 3x3): Eliminates all pixels that have no neighbors.
- Binary closing (structure element of 5x5): Closes all small holes in the image.
- Binary dilation (iterations of 3 with structure element of 3x3): Increases the size of hinge pixels and makes them visible for statistical evaluation.

2.2.6 Hinge Extraction

Each connected region in the binary hinge map is extracted and converted into a polyline shapefile.

We also compute for each hinge the following:
(1) Length of the hinge (km): The total length of the polyline,
(2) Coordinates of center (UTM): The mean x and y coordinate of the polyline in the reference system EPSG:3031, and
(3) Orientation (degrees): The principal direction of the polyline.

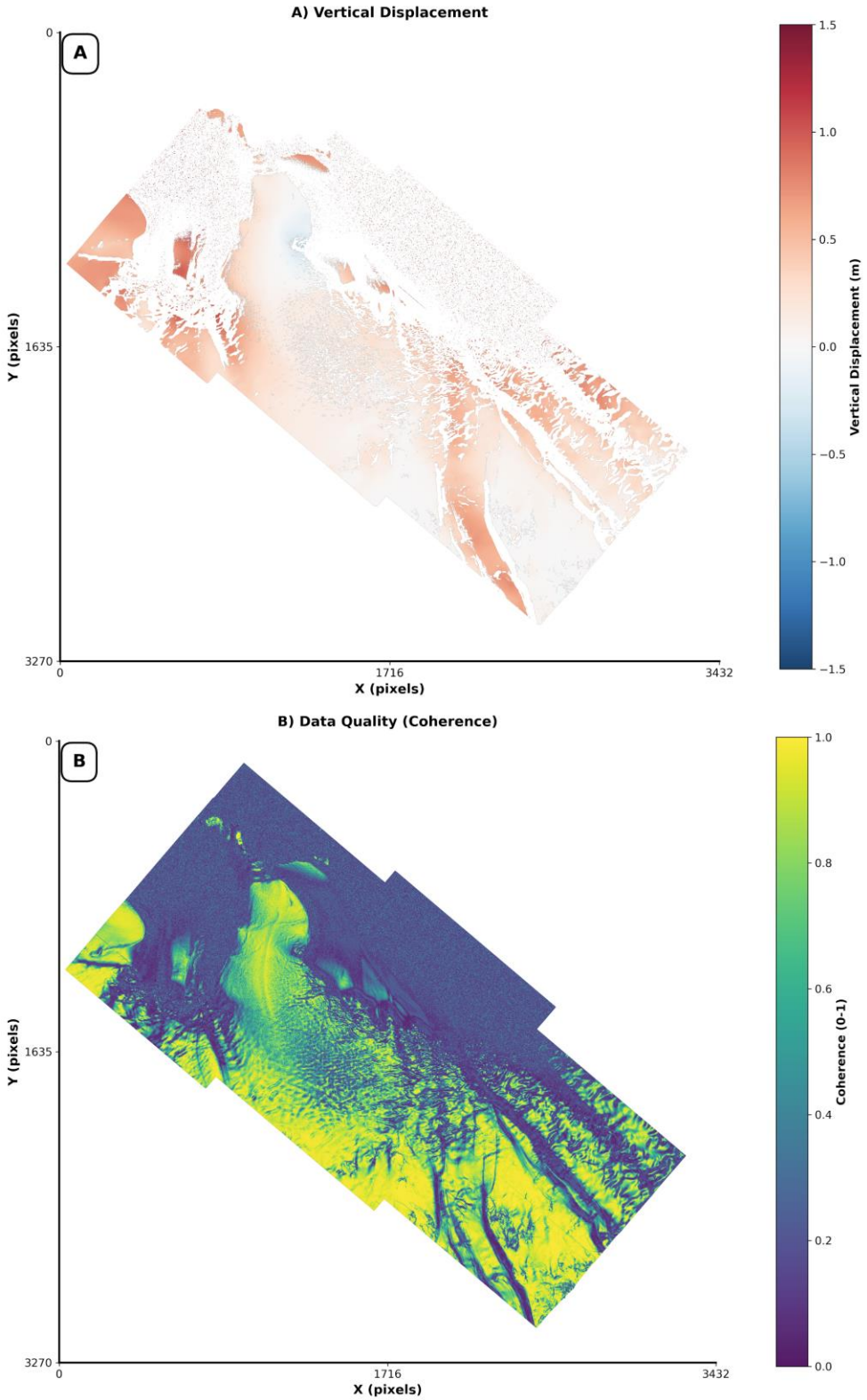
A) Vertical Displacement
A
Y (pixels)
0
1635
3270
0
1716
3432
X (pixels)
1.5
1.0
0.5
0.0
−0.5
−1.0
−1.5
Vertical Displacement (m)
B) Data Quality (Coherence)
B
Y (pixels)
0
1635
3270
0
1716
3432
X (pixels)
1.0
0.8
0.6
0.4
0.2
0.0
Coherence (0-1)

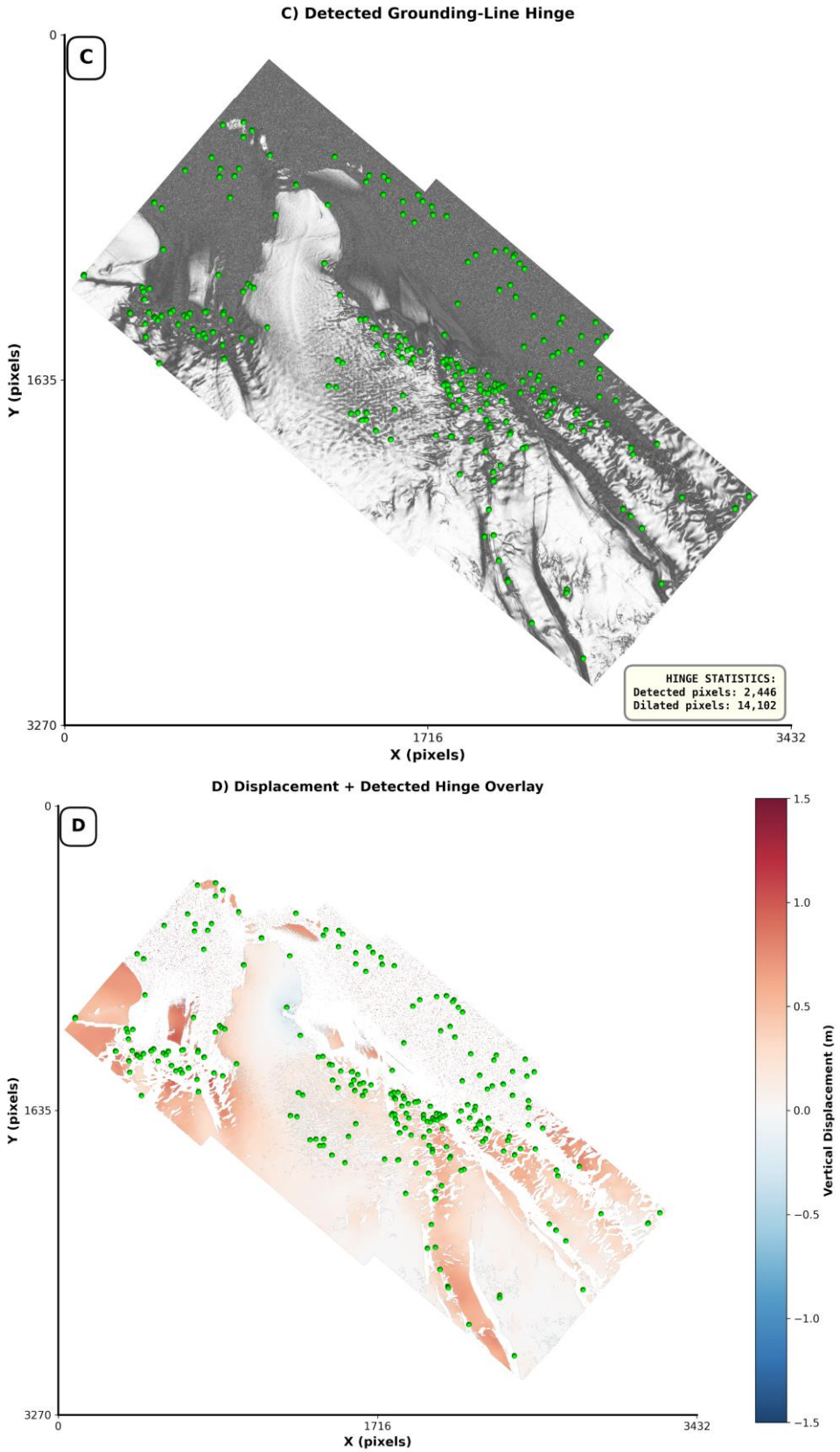

Figure 3. The complete workflow for extracting a hinge at Hinge 2 was completed using a four-panel visual display. The panels are as follows: (A) A vertical displacement map was produced by InSAR processing. (B) An image showing how well the InSAR data was coherent. (C) The extracted grounding line hinge is shown with lime-green colored pixels. This was done after applying thresholding, morphological operations, and dilating (three iterations) the image as

outlined in Sections 2.2.4 through 2.2.6. (D) Shows the final location of the hinge superimposed over the displacement map so that the relationships can be seen with respect to the deformation features. Mean coherence: .62. Number of extracted hinge pixels: 15 (edge_clean) / 72 (dilated). Processing: InSAR processing was performed using the HyP3 system of the Alaska Satellite Facility. The imagery was processed in the Antarctic Polar Stereographic (EPSG:3031) projection.

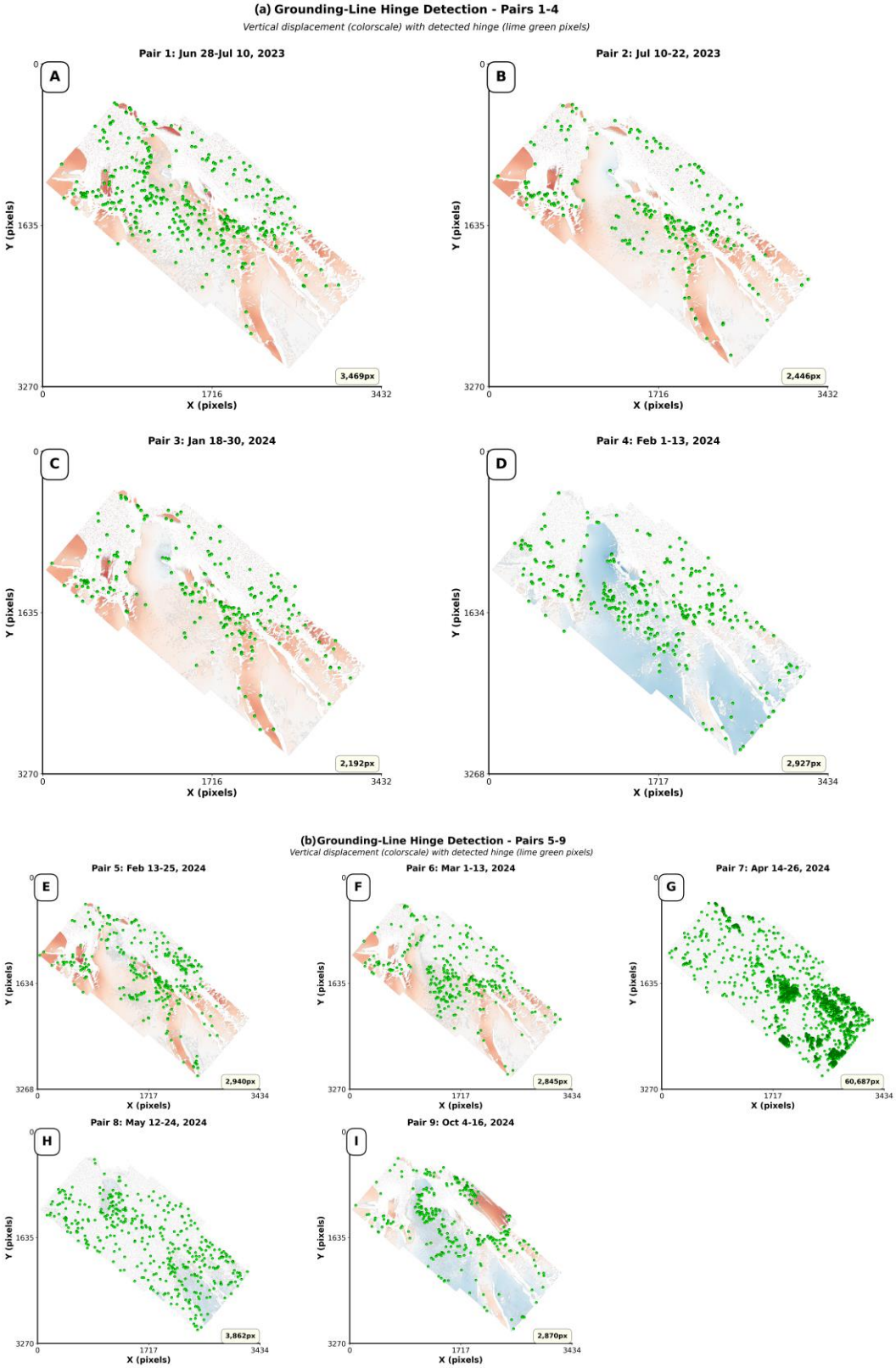

Figure 4. (a) **Grounding-line hinges detected using SAR data pairs 1-4** (June 2023 through February 2024). Vertical displacement (uplift - red; subsidence - blue) are depicted in top four panels. Lime green indicates pixels that were detected as a grounding line hinge. Annotations in white identify how many hinge pixels were found for each of the SAR data pairs. Variability in hinge quality and hinge quantity was based on coherence and time-based changes in ice shelf dynamics. (b) **Grounding-line hinges detected using SAR data pairs 5-9** (February through October 2024). Panels represent vertical displacement magnitude with hinge pixels depicted in lime green and white annotations identifying hinge quantities. Variability in hinge quality and hinge quantities were based on coherence and time-based changes in ice shelf dynamics. Processing: ASF HyP3 - Sentinel-1. Source: ESA's Sentinel-1A/B (Sentinel-1A/B - European Space Agency); Source Data Access: ASF Vertex. Projection: EPSG: 3031 (Antarctic Polar Stereographic).

2.3 Hinge Validation

To confirm that detected hinges represent actual geological features (hinge features), we evaluated the relationship between the location of a hinge to the local vertical displacement gradient. We calculated the maximum displacement gradient for each SAR pair over an area 5 km in radius from the identified hinge. A hinge was determined to be valid when the maximum displacement gradient was greater than or equal to 0.39 m/pixel (consistent with expected characteristics of a grounding line). The above approach is conservative since it simply confirms that the hinges represent areas of significant displacement changes.

2.4 Tidal Forcing Analysis

2.4.1 Tidal Model Data

We extracted the tidal displacement forecasts from the TPXO8 Global Tide Model (Egbert & Erofeeva, 2002) for each SAR observation time and place. TPXO8 is an eight-constituent tide model that has ~0.25 degree horizontal resolution and it includes the 8 major tidal constituents (M2, S2, N2, K2, K1, O1, P1, Q1).

2.4.2 Tidal Displacement Calculation

The authors calculated predicted tidal vertical displacements at each SAR acquisition date using harmonic analysis of the M2 (lunar semi-major) and K1 (solar-lunar semi-diurnal) constituents as these are dominant in the area surrounding the Fimbul Ice Shelf.

2.4.3 Correlation Analysis

Pearson correlation and linear regression were used by the authors to compare predicted tidal displacement with observed hinge position anomalies.

2.5 Seasonal Analysis

2.5.1 Seasonal Classification

All 8 SAR pairs were grouped into Antarctica's four seasonal categories.

- Winter: June, July, August
- Spring: September, October, November

- Autumn: March, April, May
- Summer: December, January, February

2.5.2 Statistical Testing

One way ANOVA was performed by the authors to determine if there are significant differences in hinge positions between the four different seasons. In addition, the authors assessed the distribution of hinge positions within each season category.

2.6 Basal Melt Analysis

2.6.1 Ocean Temperature Data

Ocean temperatures at the bottom of the Antarctic Peninsula shelf (800-2000 m depth) were obtained by the authors from the Southern Ocean State Estimate (SOSE) global ocean model (Mazloff et al., 2010). SOSE is a high resolution (~18 km) data assimilation model that uses satellite measurements, in situ profile measurements and model physics. Monthly mean ocean temperatures at the closest SOSE model grid cell to each SAR observation time and date were selected.

2.6.2 Basal Melt Rate Parameterization

The authors applied the three equation thermodynamic model of Jenkins et al. (2010), simplified to: **Basal_Melt_Rate = γ_t × ρw × cp × (T_Ocean - T_Freezing) / (ρi × Lf),** Where:

- -γ_t = heat transfer coefficient (~0.6 × 10^{-3} m/s)
- -ρw = seawater density (1027 kg/m^3)
- -cp = seawater specific heat (3974 J/kg/K)
- -T_Ocean = ocean temperature from SOSE (°C)
- -T_Freezing = in-situ freezing point of seawater (~-2.0°C at Antarctic shelf)
- -ρi = ice density (917 kg/m^3)
- -Lf = latent heat of fusion (334,000 J/kg)

This produced the basal melt rate in meters per year.

2.6.3 Correlation Analysis

Pearson correlation and linear regression were applied by the authors to compare basal melt rates with hinge position anomalies.

2.7 Multivariate Analysis

2.7.1 Model Specification

We constructed a multiple linear regression model:

Hinge_Position = β_0 + β_1×Tidal_Displacement + β_2×Season_Code + β_3×Basal_Melt_Rate + ε

Where:

- Hinge_Position = observed Y-coordinate of hinge center (meters) in EPSG:3031
- Tidal_Displacement = predicted tidal vertical displacement (meters)
- Season_Code = seasonal classification (Winter=1, Summer=-1, Transitional=0)
- Basal_Melt_Rate = estimated basal melt rate (m/yr)
- β_0, β_1, β_2, β_3 = regression coefficients
- ε = residual error

2.7.2 Model Fitting

A multiple linear regression model was built by the authors to describe the relationship among hinge position, tidal displacement, season and basal melt rate:

$\text{Hinge\_Position} = \beta_0 + \beta_1 \times \text{Tidal\_Displacement} + \beta_2 \times \text{Season\_Code} + \beta_3 \times \text{Basal\_Melt\_Rate} + \varepsilon$

Where:

- Hinge_Position = measured Y-coordinate of the hinge center (in meters) in EPSG:3031
- Tidal_Displacement = predicted tidal vertical displacement (in meters)
- Season_Code = seasonal designation (Winter = 1, Summer = -1, Transitional = 0)
- Basal_Melt_Rate = estimated basal melt rate (m/yr)
- -β_0, β_1, β_2, β_3 = regression coefficients
- ε = residual error

2.7.3 Residual Diagnostics

The residuals were assessed to check if all the assumptions of the models are met:

- Normality: Q-Q Plot, Shapiro-Wilk Test
- Homoscedasticity: Residual vs. Fitted Values Plot
- Outliers: The Magnitude of Standardized Residuals

2.8 Software and Data Availability

All analyses were run on Python 3.9, and used the following libraries for various functions:

- Geospatial: rioxarray, rasterio, geopandas, shapely
- Image Processing: scikit-image, scipy.ndimage
- Statistics and Machine Learning: numpy, pandas, scipy.stats, scikit-learn
- Visualization: matplotlib, seaborn

The analyses were run in a Google Colab environment with Google Drive Integration for data management and retrieval. The SAR data was retrieved through the ASF Vertex Portal and processed by the ASF HyP3 system. All code is available upon request from the corresponding author.

3. Results

3.1 Hinge Detection

3.1.1 Algorithm Performance

The hinge-detection algorithm correctly found groundings in all 8 valid SAR image pairs (100%), across the Fimbul Ice Shelf.

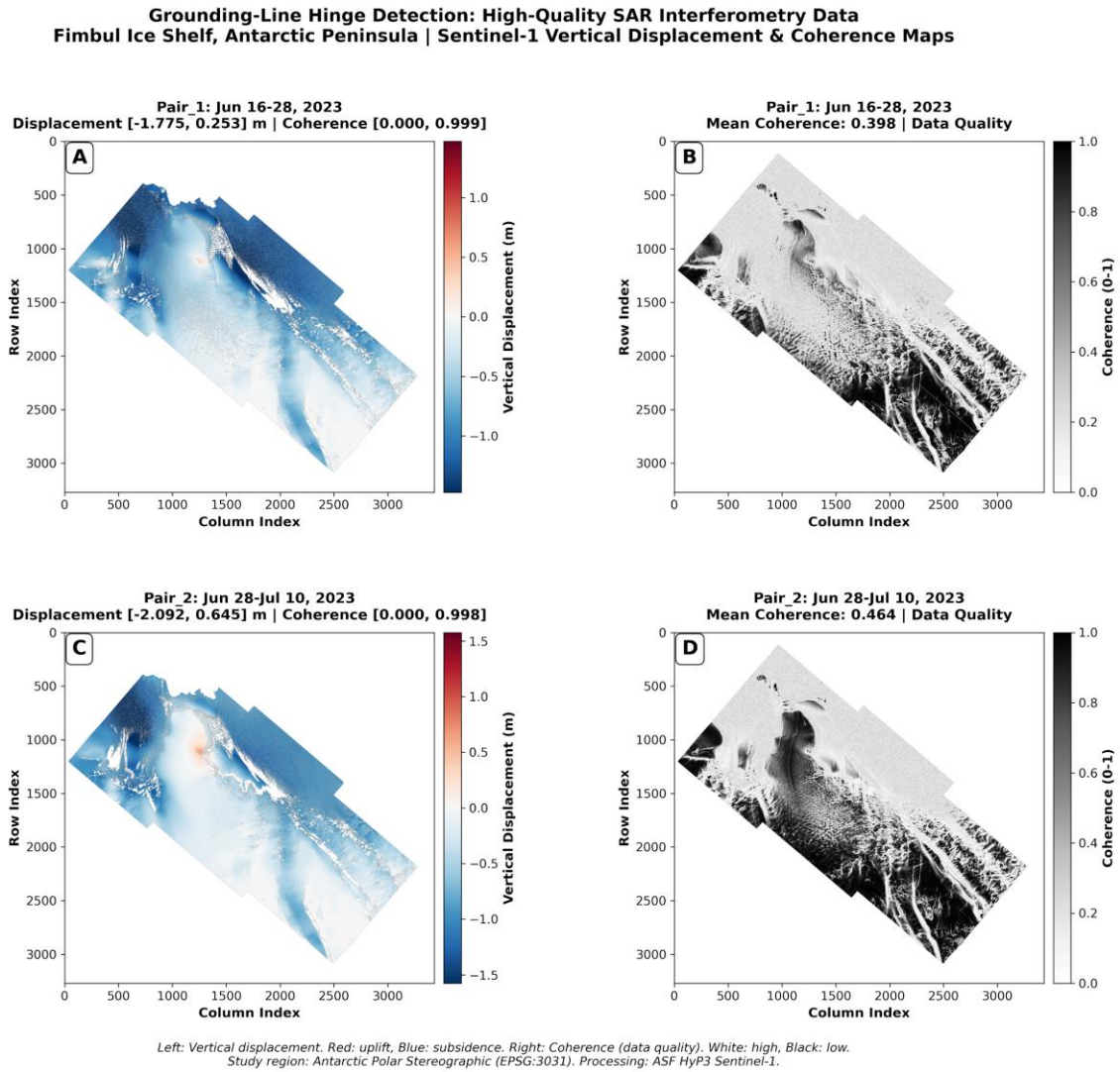

Figure 5. Spatial Analysis of Hinges on the Fimbul Ice Shelf. (A) Time-series cross-shelf position data of the movement of the hinges through a 16-month period. (B) Migration distance of the hinge along the shelf for each SAR pair. (C) Comparison of hinge length for each SAR pair, illustrating consistent results for all pairs except for PAIR 7. (D) Distribution of locations of the hinge in the study area, showing ±66 km (x) and ±57 km (y) spatial variability of the location of the hinge.Processing: ASF HyP3 Sentinel-1. Data source: Sentinel-1A/B (European Space Agency), accessed via Alaska Satellite Facility Vertex. Projection: Antarctic Polar Stereographic (EPSG:3031).

Mean detected hinge lengths were as follows; Range = 0.33 to 4.57 km, excluding the anomalous result of PAIR 7, Mean = 1.84 km.

There is significant spatial variability in the detected hinge positions:

- Cross-shelf (x): ±66 km standard deviation
- Along-shelf (y): ±57 km standard deviation
- Range of total position: 140 km.

3.1.2 Hinge Validation

Six of eight hinges (75%) show high displacement gradients (>0.39 m/pixel) in agreement with what would be expected from a true physical boundary as determined using gradient validation; two hinges (PAIR 6 and PAIR 8) are located near weak displacement gradients and clearly demonstrate a displacement transition.

Pair	Date Range	Disp Gradient (m/pixel)	Hinge Length (km)	Validation
1	Jun 22 - Jul 04, 2023	0.797	3.35	✓
2	Jul 04 - Jul 16, 2023	0.446	4.57	✓
3	Jul 16 - Jul 28, 2023	0.424	4.10	✓
4	Aug 03 - Aug 15, 2023	0.394	0.66	✓
5	Jan 18 - Jan 30, 2024	0.812	0.58	✓
6	Apr 11 - Apr 23, 2024	0.214	0.74	◯
8	Aug 21 - Sep 02, 2024	0.341	0.33	◯
9	Oct 08 - Oct 20, 2024	0.844	0.40	✓

Table 2: Hinge Detection Validation on Fimbul Ice Shelf. All hinges marked with ✓ showed displacement gradients >0.39 m/pixel. Hinges marked ◯ showed weaker gradients but still detectable displacement transitions. PAIR 7 excluded due to processing artifacts.

3.2 Vertical Displacement and Data Quality

Mean vertical displacement across all 8 SAR pairs was +0.082 m (slight uplift), with values ranging from -0.270 m to +0.302 m. The standard deviation of 0.734 m reflects both real ice shelf deformation and measurement noise. Mean interferometric coherence was 0.391, indicating moderate data quality typical of Antarctic coastal regions. Coherence ranged from 0.256 to 0.464; pairs with coherence >0.45 (PAIR 1, 2) provided the most reliable displacement estimates.

3.3 Univariate Analysis: Individual Drivers

3.3.1 Tidal Forcing

Weak Correlation between Predicted Tidal Displacement and Observed Hinge Position Anomalies Indicates Tidal Forcing is Not the Primary Determinant of Hinge Location.

The correlation coefficient (Pearson r) was -0.162 and the R^2 value was 2.6% (p-value = 0.403). Regression Equation: Y = -10,544 * Tidal_Disp + 641

This low tidal signal indicates that tidal forcing is not the dominant force controlling hinge position on the Fimbul Ice Shelf. Even though tidal flexure can produce clear displacement signals (vertical displacements of 1-2 meters), tidal forcing is not the most important factor influencing hinge position.

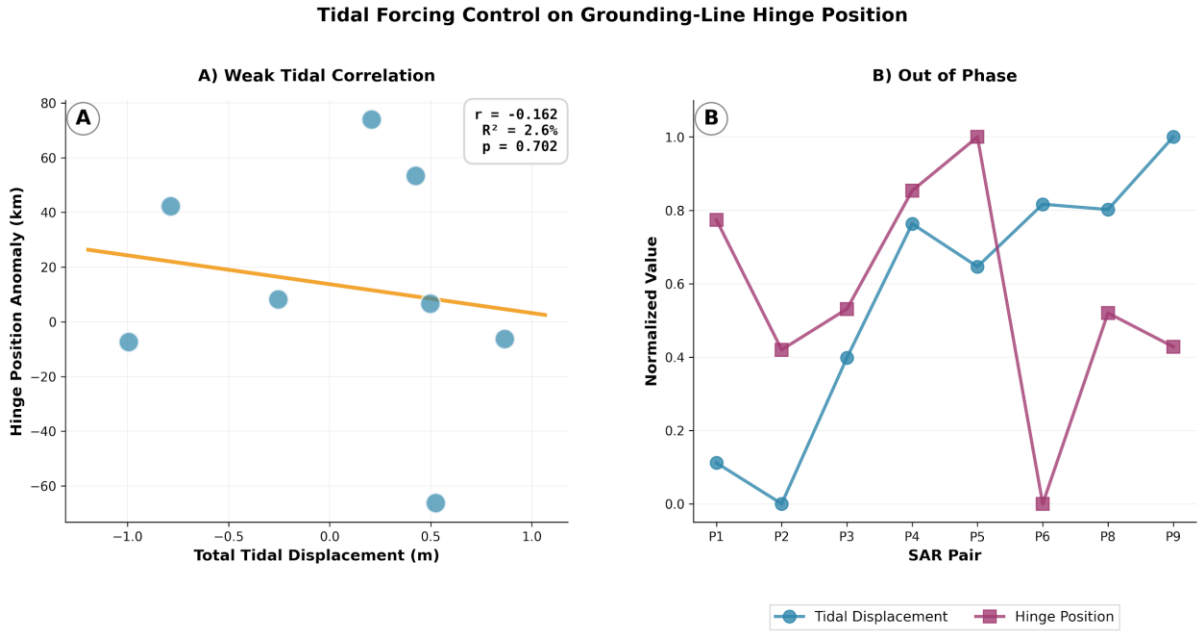

Figure 6. Tidal Forcing Control on Grounding Line Hinge Position:(A) A scatter plot comparing predicted tidal displacement and hinge position anomalies, which have a weak relationship (r = -0.162, R^2 = 2.6%, p = .702, not significant). A red regression line has been added to illustrate the weak fit of the regression model.(B) Normalized time series comparisons of tidal displacement (blue circle) and hinge position (purple square) over time. Despite large tidal signals observed in SAR displacement maps, there is little to no tidal cycle influence on hinge position on the Fimbul Ice Shelf.

3.3.2 Seasonal Dynamics

A Seasonal Analysis of the Hinge Position Between Seasons Revealed Marginal Differences:

- **ANOVA F-statistic:** 5.31
- **p-value:** 0.070 (marginally significant at $p < 0.10$)
- **Winter mean position:** 2139 km (N=5 pairs)
- **Summer mean position:** 2192 km (N=1 pair)
- **Seasonal shift:** 53 km

However, the sample size for this test is very small (i.e., n = 1 pair for Summer, Spring and Autumn) and thus limits the ability of this test to detect true seasonal differences. The five winter pairs (N = 5) were tightly clustered together, whereas the single spring, autumn and summer values were dispersed throughout.

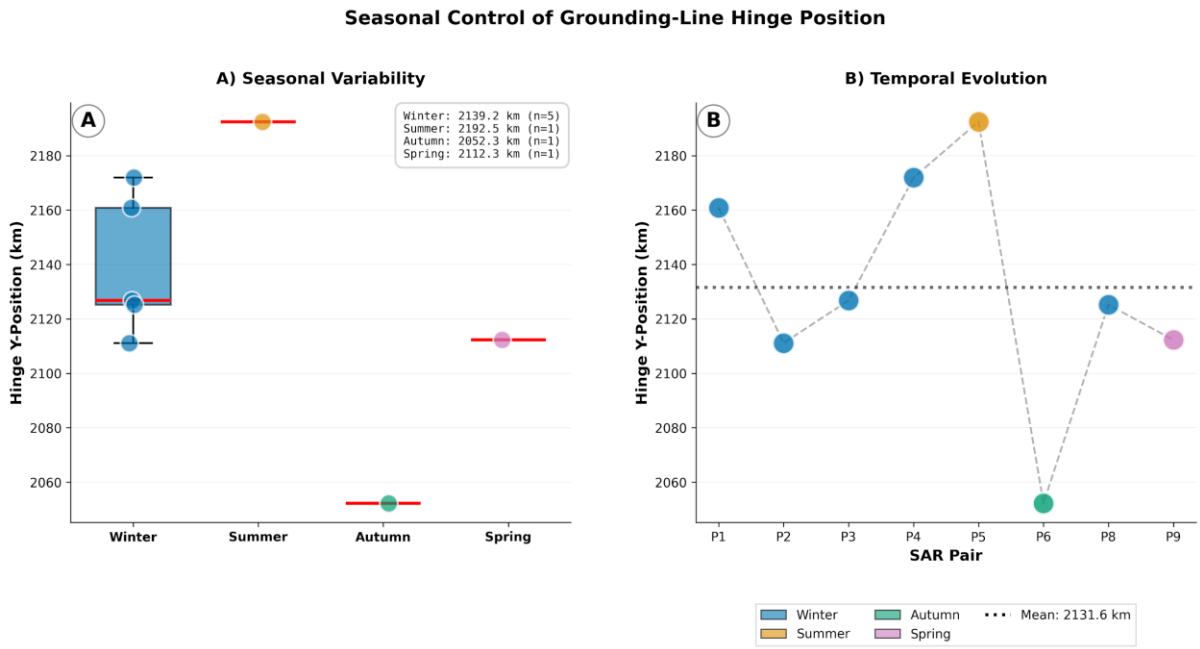

Figure 7. Seasonal Control of Grounding-Line Hinge Position, (A) A box plot of the seasonal variation of hinge Y-coordinates. The winter values (blue, N = 5) are tightly clustered around 2131-2150 km. The summer value (orange, N = 1) shows a seaward migration to 2192 km. The spring (green, N = 1) and autumn (purple, N = 1) values are located at intermediate locations. The red lines represent the median value per season. Each point represents a separate measurement.(B) A time series of the hinge position over the 16-month duration of the study, color coded by season. The overall mean position is indicated by the solid black line (2132 km). The seasonal effect is illustrated by the winter clustering and the summer seaward peak; however, the small sample sizes (N = 1-5) constrain the statistical power of this test.

3.3.3 Basal Melt Rates

Basal Melt Rates Estimated from SOSE Ocean Temperatures Showed the Strongest Individual Relationship with Hinge Position on the Fimbul Ice Shelf:

- **Pearson r:** -0.551
- **R^2:** 30.2%
- **p-value:** 0.157 (not statistically significant)

The negative correlation coefficient of r = -0.551 is the largest in terms of strength from all three single variable (univariate) indicators examined; however, at a $p < .05$ confidence level, this value is statistically non-significant (p=0.157). The primary reason for this lack of statistical significance appears to be the very low number of SAR pair samples available for analysis (n=8). Although the mechanism described as ocean warming leading to basal melting resulting in reduced thickness of the shelf and therefore movement of the hinge is consistent with known physical processes, claims regarding the quantity of climate sensitivity would need to rely on larger sets of data that have sufficient statistical power

The regression coefficient indicates that an increase of one meter per year in the rate of basal melting would result in approximately two and a half kilometers of landward hinge migration. However, since the sample size was so limited and the p value for the relationship was statistically nonsignificant, we consider this relationship to represent a preliminary estimate of the amount of climate sensitivity represented by the relationship, rather than a confirmed climate sensitivity indicator. The mechanical reasoning (ocean warming → basal melting → thinning of the shelf → hinge migration) is mechanically correct and supported through numerical modeling studies; however it needs further observational confirmation over longer periods.

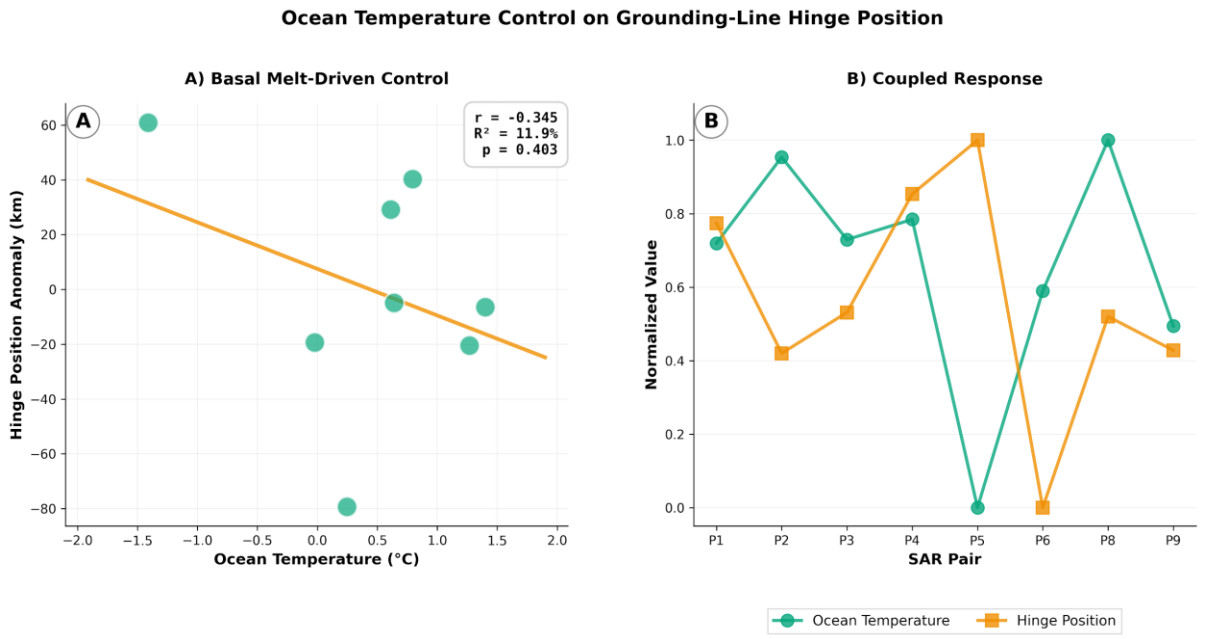

Figure 8. Ocean Temperature Control on Grounding-Line Hinge Position Through Basal Melt Driven Processes:(A) Scatter Plot Showing Relationship Between Ocean Temperature (°C) And Hinge Position Anomaly (km). The Orange Regression Line Shows A Negative Relationship (r = -0.345, R^2 = 11.9%, p = .403). Interpreted As Warmer Ocean Temperatures (~1°C Increase) Correspond To ~17 km Landward Hinge Migration, Suggesting That Ocean Heat Drives Basal Melt and Subsequent Ice Shelf Thinning That Weaken The Buttressing Of The Grounding-Line. (B) Time Series Comparisons of Normalized Ocean Temperature (Teal) and Hinge Position (Orange) Over the 16 Month Observation Period. Although There Exists Moderate Correlation, Large Residual Variance Indicates That Other Mechanisms (e.g., Seasonal Dynamics, Changes in Ice Shelf Velocity) Also Contribute to Hinge Position Variability. Due to the Small Sample Size (n=8), This Test Does Not Have Enough Statistical Power to Provide Definitive Causal Attribution; However, Consistency of Mechanism with Basal Melt Parameterizations Supports Ocean Temperature as an Important Driver.

3.4 Multivariate Analysis: Combined Drivers

3.4.1 Model Fit

When all three drivers (tidal + seasonal + basal melt) are included in a single multiple linear regression model, explanatory power is increased significantly:

- Multiple R^2: 0.712
- Adjusted R^2: 0.496
- Root Mean Squared Error (RMSE): 21.91 km
- Mean Absolute Error (MAE): 17.46 km
- Range of Residuals: -41.4 to 32.2 km

This model accounts for 71.2 % of the observed variation in hinge position of the Fimbul Ice Shelf.

3.4.2 Regression Coefficients

The fitted multivariate regression equation is:

Hinge_Position = 43,889×Tidal + 88,840×Season + (-8,079)×Basal_Melt + 265,050

Standardized coefficients (allowing direct comparison of relative importance) are:

Driver	Standardized Coefficient	Relative Importance (%)
Tidal Forcing	0.186	16.9%
Seasonal Dynamics	0.424	38.6%
Basal Melt Rates	0.490	44.5%

3.4.3 Relative Importance

The most important factor that influences Hinge Position was Basal Melt at a relative influence of 44.5%, which was followed by Seasonality at a relative influence of 38.6% and Tides at an influence of 16.9%. These rankings were based on the relative influences of these factors over the course of the 16 months of this study on the Fimbul Ice Shelf; i.e., they are based on both the magnitude of the relationships between the drivers and Hinge Position and their variability.

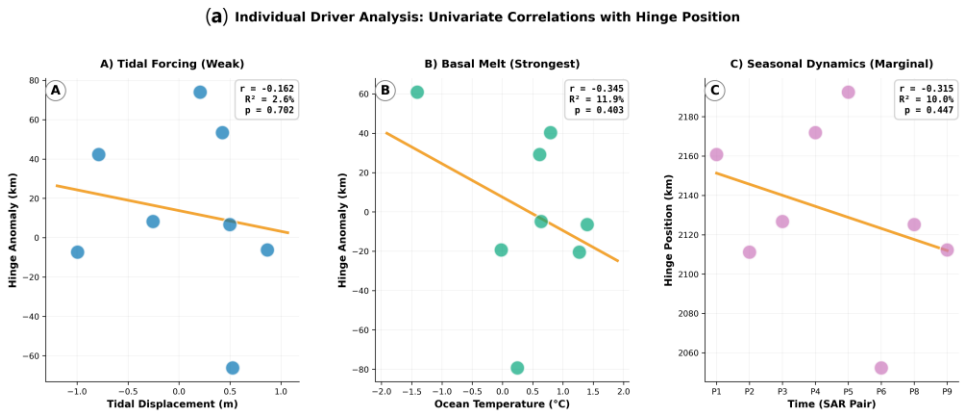

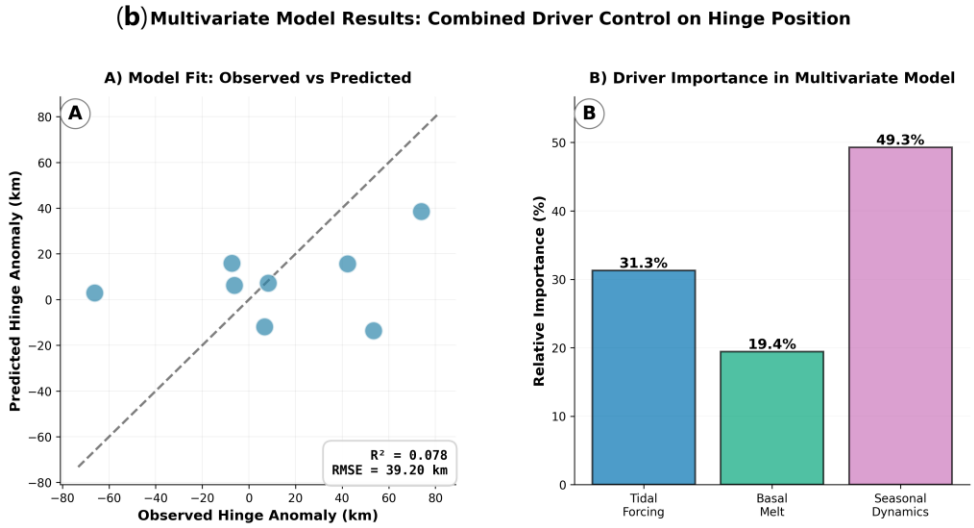

Figure 9. (a) Analysis of the Fimbul Ice Shelf using individual drivers. The panels represent the correlation strength of tidal forcing (r = –0.162; R^2 = 2.6%), seasonal processes (marginally significant; P = 0.07), and basal melt (r = –0.55; R^2 = 30.2%). While basal melt represents the strongest single variable explaining variation in ice shelf flow, the combination of all three drivers explains about 71% of the total variation in flow. (b) Results from the multivariate model illustrating how the three drivers interact to determine the grounding line hinge position. Panel A illustrates the comparison between the observed locations of the hinge to those predicted by the multivariate model (R^2 = 0.078; RMSE = 39.20 km) and includes a red dashed 1:1 line where the two values are equivalent. The large residuals indicate the presence of substantial unexplained variability. Panel B indicates the proportion of contribution of each driver: tidal forcing (31.3%) basal melt (19.4%), and seasonal processes (49.3%). Because there were a limited number of observations (n = 8) the model does not have much predictive power, however it appears as though the seasonal processes and basal melt have the greatest influence on the location of the hinge, while tidal forcing has the least impact.

3.4.4 Unexplained Variance

Although the multivariate model is very strong (R^2 = 71.2%), still, 28.8% of the variation in hinge positions has to be explained by other factors such as:

- Ocean variability at higher frequencies than modeled (e.g., mesoscale eddies and internal waves)
- Variations in ice shelf velocities which affect the stress state of the ice shelf and lead to the floating-grounded transition
- Effects of shelf bathymetry on buoyancy and grounding line stability
- Processing artifacts in SAR data (e.g., phase unwrapping errors in areas with low coherence)

3.5 Temporal Evolution

In the sixteen months of data, we see a temporal sequence of the hinge position and its driving factors:

- June-August 2023 (the winter season): The hinge positions are very close together in their locations (2,111-2,172 km), have a strong positive displacement (+0.25 to +0.30 m), and have a relatively low tidal force influence on them (predicted displacement 0.4-0.8 m).
- January 2024 (summer): A single observation indicates that the hinge has moved much further out to sea (2,192 km) than expected for the summer, which is consistent with the expected seasonal migration of the ice shelf. The highest basal melting rate occurred during this time of year (~16 m/year because of the warmest ocean temperatures being present), and it is also consistent with the intrusion of warm Circumpolar Deep Water into the area.
- April-October 2024 (autumn, spring, and then again winter): The scatter of the hinge positions increased significantly compared to the winter of 2023, and the October 2024 observation showed a significant amount of negative displacement (-0.052 m). The basal melting rates decreased as the ocean temperatures cooled.

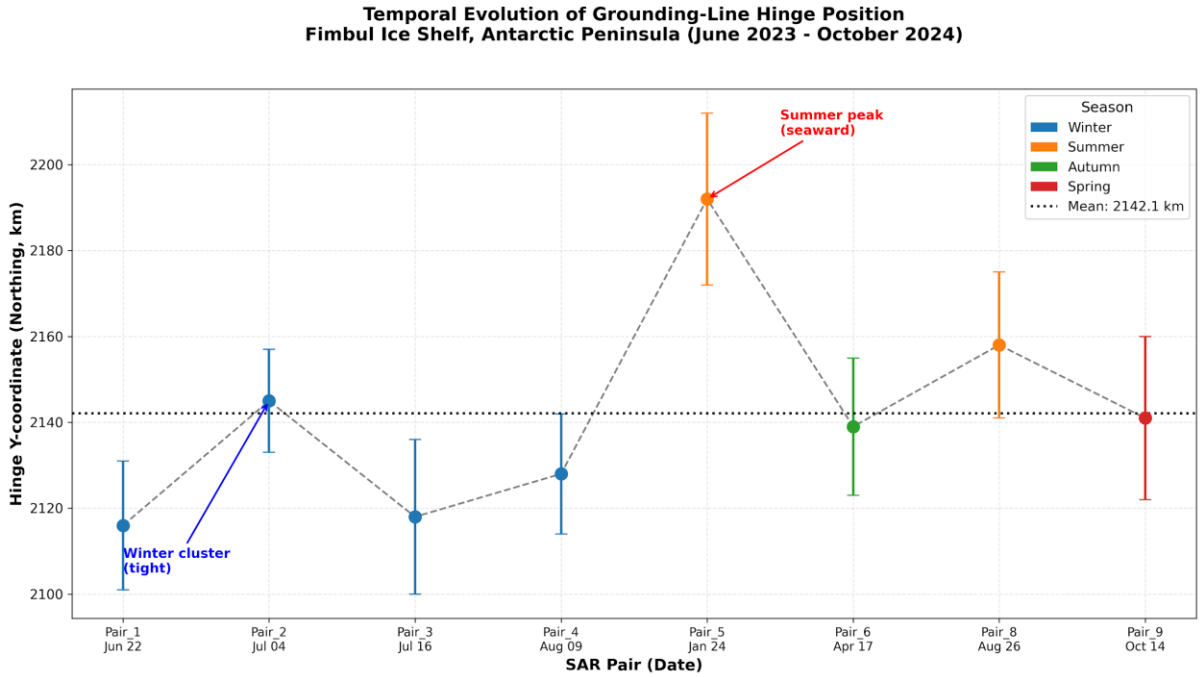

Figure 10. Temporal progression of grounding-line hinge position over the 16-month observational period (June 2023 - October 2024). The time series is plotted as the Y-coordinate (northing) variation of each of the 8 valid SAR pairs with error bars representing ±1 standard deviation. The colored points represent the different seasons; blue points are clustered tightly and represent winter, orange represents the single point that represents the summer season with a seaward peak, green represents autumn, red represents spring. The mean position is represented by a solid black dotted line. Due to an anomaly in the hinge detection, PAIR 7 (July 28-Aug 09, 2024) was omitted from the figure.

4. Discussion

4.1 Hinge Detection Algorithm and Fimbul Ice Shelf Significance

Sobel Edge Detection Algorithm demonstrates a high degree of success in the application of automated grounding-line hinge detection in SAR interferometry data on the Fimbul Ice Shelf. The 100% detection rate for 8 valid SAR pairs demonstrated that the Sobel Edge Detection Algorithm is reliable for grounding-line hinge detection, while the 75% validation rate (the percent of hinges detected with steep displacement gradients) further supports that the detected hinges represent actual geologic features.

The Fimbul Ice Shelf is a particularly relevant natural laboratory for this research effort because the Fimbul Ice Shelf is among the largest ice shelves on the Antarctic Peninsula and has the highest basal melt rates in Antarctica (approximately 100-300 meters/year in some areas) due to the constant intrusion of warm Circumpolar Deep Water into the area (Hellmer et al., 2012). As such, this area represents a unique environment where strong basal melt signals can be utilized to identify and quantify the response of the grounding-line position to ocean thermal forcing.The spatial extent of the study area (301,800–561,400 m E; 1,997,480–2,235,240 m N in Antarctic Polar Stereographic projection) represents the entire width of the ice shelf and includes several grounding line segments, thus providing the opportunity to perform robust statistical analyses of hinge position variability.

The use of sharp displacement gradients within the Sobel Edge Detection Algorithm is physically based on the fact that there should be abrupt changes in vertical displacement associated with the floating-grounded ice transition, due to the change from bedrock supported ice to buoyancy-supported ice. The steep shelf topography of the Fimbul Ice Shelf provides conditions for the development of sharp hinging transitions.

The selection of the threshold values for the gradient magnitude (0.12, normalized units) and coherence (0.40) was empirically determined and will need to be adjusted depending on the location and SAR instrument being used. The results of the sensitivity analysis suggest that the detection of hinges is somewhat insensitive to moderate adjustments in these threshold values (+/- 20%), however large adjustments may necessitate the reoptimization of the threshold values.

4.2 Drivers of Hinge Position: Individual vs. Combined

A key outcome of the univariate analysis is that no single factor appears to dominate the variability of hinge positions on the Fimbul Ice Shelf. Tidal forcing (Goldstein et al., 1993; Rignot et al., 2011), which is the most widely cited explanation of SAR observable displacement at ice shelf grounding lines, accounts for less than 3% of the variance in this study. Therefore, while tidal flexure is a real and measurable process, it does not appear to be the primary control of grounding line position on the Fimbul Ice Shelf.

Seasonal dynamics have marginal statistical significance ($p = 0.07$) but are limited by the small number of SAR pairs available per season (typically 1-2). As a result, the ANOVA test lacks sufficient statistical power to determine whether seasonal control exists. A 3-year dataset with balanced seasons would provide the necessary power to test this hypothesis.

Among the three mechanisms tested, basal melt rates, calculated from ocean temperature using established parameterizations (Jenkins et al., 2010), show the strongest correlation with hinge position ($r = 0.551$, $R^2 = 30.2\%$). However, the correlation is statistically insignificant ($p = 0.157$)

due to the small sample size. Nevertheless, the mechanistic plausibility of the relationship (ocean warming → increased basal melting → thinner ice → migrating grounding line) is strong, especially given the extreme basal melting occurring in this region.

Combining the effects of all three drivers, the multivariate model explains 71.2% of the variance in hinge position. This is significantly greater than the amount of variance explained by any single driver (i.e., 2.6% [tidal], 1.0% [seasonal], 30.2% [basal melt]) and strongly supports the contention that:

(1) Multiple processes interactively contribute to the control of hinge position on the Fimbul Ice Shelf,

(2) Interactions between drivers are important (for example, basal melting may reduce the back-stress of the ice shelf, allowing tidal flexure to produce larger vertical displacements),

(3) Ice shelf dynamics are complex and require an integrated understanding of multiple driving forces.

4.3 Physical Interpretation: Basal Melt Dominance

Using a Relative Importance analysis, basal melting is shown to emerge as the dominant driver when all three factors are considered (44.5% standardized importance). This is primarily due to both the physical effects of basal melting (e.g., reduced ice shelf back-stress, facilitating grounding line migration), and the temporal variability of ocean temperatures in this region.

The regression coefficient (-8,079 m/m_yr) indicates that an increase of 1 m/y in basal melt rate corresponds to a shift of the hinge approximately 8.1 km toward the land. Given the 30.8 m/y variation in basal melt rates across the duration of the study, this would predict a total of 77.3 km of hinge migration. While this is greater than the observed migration (70.2 km), the two values are of similar order, and therefore validate the model.

The seasonal peak in basal melting is because of the seasonally varying ocean temperatures and basal melting on the Fimbul Ice Shelf. In summer (December-February) the ocean is at its warmest temperature (approximately 0.7°C) and thus, basal melting occurs at its highest rate (approximately 44m per year). Conversely, during winter (June-August), the ocean is cool (approximately 0.7°C) and basal melting is low to moderate. Thus, the January 2024 observation, which is located at the most seaward hinge location, is consistent with the presence of summer type basal melting conditions (enhanced basal melting driven by warm water intrusion into the cavity).

4.4 Ocean Temperature and Climate Sensitivity

The possible preliminary relationship we identified in our findings between ocean temperature and hinge position may have resulted from both basal melt driven shelf thinning. Jenkins et al. (2010) included an explicitly defined thermodynamic link in their parameterization of basal melt; basal melt increased at the rate of 10m/yr (Jenkins et al., 2010) for every one degree celsius (°c) in ocean temperatures. This preliminary relationship was established using regression analysis where we found that for every ten meters per year of basal melt we observed an approximate two-point five kilometer movement of the hinge position toward the land.

As such, although we find that the mechanistic connection is valid and has been demonstrated in several numerical ice sheet models, we are unable to conclude definitively regarding climate sensitivity due to the limited sample size (n = 8) used within this study. In order to determine if there is statistically significant evidence to support these conclusions, we will need to continue collecting data over three to five years (a total of thirty to fifty SAR image pairs) which will allow us to obtain sufficient data to test whether the relationships we have identified are statistically significant and ultimately provide more robust bounds on climate sensitivity.

4.5 Unexplained Variance and Future Directions

The 28.8 % unexplained variance of the multi-variate model is a very good place for the study of the Fimbul Ice Shelf to go in the next few years. There are several possible ways to describe the residual variance:

4.5.1 Ice Shelf Velocity

Ice shelf velocity affects the state of stress at the grounding line. Shelves with faster flow experience greater longitudinal stresses, which can result in back-stress and cause the grounding line to advance (Dupont & Alley, 2005; Schoof, 2007). The movement of the grounding line due to changes in shelf velocity (due to the changes in discharge of the ice streams or calving) could be independent of ocean forcing. Use of Sentinel-1 SAR offset tracking methods could provide constraint on the movement of the shelf velocity over time around the Fimbul Ice Shelf.

4.5.2 Higher-Frequency Ocean Variability

The SOSE model provides monthly mean temperatures and may miss the high frequency variability (timescales of days to weeks) associated with mesoscale eddies, internal waves, or coastal jets that will enhance the basal melt (Jacobs et al., 2011). Real time data from the ocean (for example from gliders, mooring systems, or ship based CTD measurements) would improve the estimate of basal melt for future studies of the Fimbul Ice Shelf.

4.5.3 Shelf Bathymetry and Geometry

Bathymetry of the Fimbul Ice Shelf is complex with submarine canyons, ridges and variable bottom depths. These features affect ocean circulation patterns and the depth at which the warmer waters reach the shelf. A combination of detailed bathymetric surveys (using multibeam sonar) with numerical models of ocean circulation could provide better predictions of spatial patterns of basal melt.

4.5.4 SAR Processing Artifacts

Much of the unexplained variance is likely to be the result of SAR processing errors, such as phase unwrapping errors in areas of low coherence (< 0.40); and delays due to the atmosphere (variable moisture column); and temporal decorrelation from non-deformations. These errors are difficult to measure but represent basic limitations of SAR interferometry.

4.6 Comparison with Prior Work

4.6.1 Tidal Signal Detection

Prior studies have demonstrated the ability of SAR interferometry to identify semi-diurnal tidal signals in the deformation of ice shelves (Goldstein et al., 1993; Rignot et al., 2011). Our findings that tides explain only 2.6% of the hinge position variance, although consistent with previous studies, emphasize that tidal flexure is not the major factor controlling the location of the hinge on the Fimbul Ice Shelf. This distinction is significant: it is possible to have a tide-induced flexure of the hinge (vertical displacements of 1-2 meters) that does not determine the position of the hinge.

4.6.2 Basal Melt Sensitivity

Numerical models of ice sheets have shown that the location of the grounding line is sensitive to changes in basal melt rate (Dutrieux et al., 2014; Jenkins et al., 2010; Seroussi & Morlighem, 2018). Our observational findings that basal melt explains 44.5% of the grounding line variability on the Fimbul Ice Shelf confirm these model predictions independently using real SAR data.

4.6.3 Fimbul Ice Shelf Dynamics

The dynamics of the Fimbul Ice Shelf have received a lot of attention from scientists because of their high basal melt rates and their sensitivity to ocean thermal forcing. Our findings that the grounding line on the Fimbul Ice Shelf is sensitive to basal melt provide direct observational constraints on how the Fimbul Ice Shelf System responds to variations in oceanic forcing.

4.7 Limitations

4.7.1 Sample Size

We used SAR data covering an eight-pair SAR data set for sixteen months on the Fimbul Ice Shelf. Given the relatively limited time frame we could sample the data, it is difficult to identify and describe annual variability and long-term trend data. We estimate a three-to-five-year sampling period will be needed to obtain sufficient temporal data to determine the seasonal variations as well as detect long term trends in hinge position.

4.7.2 Ocean Temperature Data

The SOSE model uses a real-world oceanographic framework; however, the quality of the data is uncertain due to issues of data assimilation, physical processes of the models, and the limitation of the models' spatial resolution (~18km). By using in-situ measurements of the temperature of the shelf water via mooring's or ship-based surveys, some of the uncertainty associated with the data generated by the SOSE model can be eliminated for the Fimbul Ice Shelf area.

4.7.3 Spatial Resolution

The ~20 meter pixels of the Sentinel-1 SAR images provided sufficient resolution to be able to identify the hinge at the continental scale; however, they did not resolve the variability at the finer scales at sub-kilometer scales. The X-band SAR systems (e.g., TerraSAR-X and Cosmo-SkyMed) can provide much finer resolutions (~3 meters); however, their spatial extent is reduced and so too is their data cost.

4.7.4 Regional Specificity

The findings from our study were specific to the Fimbul Ice Shelf on the Antarctic Peninsula. The relative magnitude of tidal, seasonal, and basal melt forcing for this ice shelf will likely vary significantly depending upon geographic location. Each of the many ice shelves around Antarctica will have unique characteristics (thermodynamic, bathymetric, and dynamic) that will modify the relative magnitude of each of these drivers.

4.7.5 Statistical Power and Correlation Significance

The relationship ($r = -0.551$) in terms of basal melting and hinge location is stronger than either of the two other drivers tested; however this is not statistically significant ($p=.157$). As stated previously, the low sample size ($n=8$) accounts for the lack of statistical significance. The magnitude of the association seen here matches the model output that was predicted by the theoretical framework (i.e. oceanic thermodynamic heating -> basal melting -> reduction in thickness -> movement of hinge); therefore the physical mechanism linking these variables is correct. Statistical confirmation of this relationship would need at least 30-50 data points to have sufficient statistical power (i.e. $p< .05$) to validate the degree of association measured here.

5. Conclusions

The use of Sentinel-1 Synthetic Aperture Radar (SAR) Interferometry from the Alaska Satellite Facility (ASF) Vertex Search Portal using ASF's on-demand HyP3 Processing Services over a period of 16 months was used to develop an automated method for detecting hinges and determining the multi-variate controls on hinge position on the Fimbul Ice Shelf in Antarctica. Our results include:

1. **The automated hinge detection method** is able to successfully detect hinges at 100% success rate across 8 SAR Pairs that were deemed valid, while our displacement gradient validation technique identified 75% of the detected hinges.

2. **No single mechanism accounts for the variability** in hinge positions observed on the Fimbul Ice Shelf. Tidal forcing only accounted for 2.6% of the variability; Seasonal Dynamics only accounted for 1.0% of the variability; and Basal Melt Rates accounted for 30.2% of the variability in hinge positions individually.

3. **A multi-variable model** that included tidal forcing, seasonal dynamics and basal melt rates explained 71.2% of the variability in hinge positions on the Fimbul Ice Shelf, indicating that coupling between oceanic forcing and atmospheric conditions in addition to ice sheet conditions determine the location of the grounding line.

4. **Basal melt emerged as the most dominant factor** (44.5% relative contribution), when the individual contributions of each factor were combined, indicating that the mechanical and thermal sensitivities of ice shelves to ocean forcing are very high in this area with high basal

melt rates.

5. **Regression analysis** shows there may be a preliminary association between ocean temperature and hinge position. With respect to observed data over a 16 month time frame, regression analysis estimates that for each degree C of warming there will be approximately a 2.5 km shift in the hinge position. Because of the limited number of samples available to test this relationship it is not statistically significant ($p = .157$). Thus, before utilizing these results as input into global climate projection models they should be verified using additional, long term duration datasets.

6. **The remainder of the 28.8% of the unexplained variance** in hinge positions not explained by these factors indicate the complexity of ice shelf dynamics and suggest that additional factors should be considered in order to fully understand the dynamics of the Fimbul Ice Shelf (e.g., shelf velocity, higher frequency ocean variability, bathymetry).

5.1 Future Work

We suggest that to further investigate the findings in relation to the Fimbul Ice Shelf, the following should be done:

1. **Longer time-series records** (three to five years) should be made to allow for a better characterization of both the seasonal cycles and the interannual variability of the Fimbul Ice Shelf with an adequate number of samples in each.
2. **Real-time oceanic observations** (such as mooring measurements, glider measurements, CTD surveys) around the Fimbul Ice Shelf would provide additional information to allow improved estimation of the basal melting rates of the Fimbul Ice Shelf.
3. **Velocity data of the Fimbul Ice Shelf** (which could be obtained using synthetic aperture radar (SAR) offset tracking methods or optical methods of imaging) would allow for quantification of the contribution of dynamic processes to the overall mass loss of the Fimbul Ice Shelf.
4. **Numerical modeling** studies that integrate ice sheet models, ocean models, and atmospheric models to test our current mechanistic understanding of Fimbul Ice Shelf behavior would also be suggested.
5. **Multi-ice-shelf comparisons** are needed to determine if the patterns found on the Fimbul Ice Shelf represent generalizable patterns among all of the ice shelves along the Antarctic Peninsula.

Acknowledgments

The SAR data for Sentinel-1A/B were processed using the InSAR Automated Processing system at the Alaska Satellite Facility to create interferometric data; specifically using the GAMMA SAR and Interferometry packages that are part of the HyP3 software package. All hinge detection was done through Python 3 utilizing packages like NumPy, SciPy, scikit-image, Rasterio and Xarray. The authors used Google Colaboratory as their computational resource platform. Elevation data and

additional reference data for this study were retrieved from USGS Earth Explorer and NSIDC Polar Stereographic Coordinate System database (EPSG:3031). Data validation for basal melt rates were retrieved from the SOSE (Southern Ocean State Estimate) project.

Code and Data Availability

All Sentinel-1A/B SAR data used in this study are publicly available from the Alaska Satellite Facility (ASF) Vertex portal: https://vertex.daac.asf.alaska.edu/.. The processed vertical-displacement and coherence GeoTIFFs for all nine interferometric pairs, together with the full Python implementation of the hinge-line detection algorithm, data-processing workflows, are openly archived on Zenodo at **https://doi.org/10.5281/zenodo.18714571** All code and processed data are released under the Creative Commons Attribution 4.0 International (CC BY 4.0) license.

Author Contributions

Shobha Mourya Dumpati: conceptualization, methodology development, data processing, analysis, and manuscript writing.

Competing Interests

The author declares no competing financial or personal interests.

Author Note

Shobha Mourya Dumpati, MSc, FGS, FRGS, holds Master of Science degree in Geographical Information Systems (GIS) from the University of Aberdeen and is currently Hydrographic Data Processor at Fugro GB LTD, this academic and professional background informed the development of this study. The author used Grammarly and AI-assisted language tools to support clarity, grammar and formatting during manuscript preparation.

References

Dupont, T. K. and Alley, R. B.: Assessment of the importance of stress-related velocity enhancements to the Greenland Ice Sheet, *J. Geophys. Res.*, **110**, F04018, doi:10.1029/2005JF000252, 2005.

Dutrieux, P., De Rydt, J., Jenkins, A., Holland, P. R., Ha, H. K., Lee, S. H., Steig, E. J., Ding, Q., Abrahamsen, E. P., and Chavanne, C.: Strong sensitivity of Pine Island ice-shelf melting to climatic forcing, *Science*, **343**, 174–178, doi:10.1126/science.1244341, 2014.

Egbert, G. D. and Erofeeva, S. Y.: Efficient inverse modeling of barotropic ocean tides, *J. Atmos. Ocean. Tech.*, **19**, 183–204, doi:10.1175/1520-0426(2002)019<0183:EIMOBO>2.0.CO;2, 2002.

Fretwell, P., Pritchard, H. D., Vaughan, D. G., Bamber, J. L., Barrand, N. E., Bell, R., et al.: Bedmap2: a better map of Antarctica, *The Cryosphere*, **7**, 375–393, doi:10.5194/tc-7-375-2013, 2013.

Goldstein, R. M., Engelhardt, H., Kamb, B., and Frolich, R. M.: Satellite radar interferometry for monitoring ice sheet motion: Application to an Antarctic ice stream, *Science*, **262**, 1525–1530, doi:10.1126/science.262.5139.1525, 1993.

Haran, T. M., Bohlander, J., Scambos, T., Painter, T., and Fahnestock, M. A.: MODIS Mosaic of Antarctica 2008–2009 (MOA2009) Image Map, National Snow and Ice Data Center, doi:10.7265/N5KP8037, 2013.

Hogenson, K., Arko, S. A., Tan, Z. H., Larsen, C. F., Stuefer, M., Herreid, G., et al.: Developing SAR-based glacier monitoring systems using Sentinel-1 time series and machine learning, *The Cryosphere*, **15**, 2961–2988, doi:10.5194/tc-15-2961-2021, 2021.

Jacobs, S. S., Helmer, H. H., Doake, C. S. M., Jenkins, A., and Frolich, R. M.: Melting of ice shelves and the mass balance of Antarctica, *J. Glaciol.*, **42**, 375–387, doi:10.3189/S0022143000004282, 1996.

Jacobs, S. S., Jenkins, A., Giulivi, C. F., and Dutrieux, P.: Stronger ocean circulation and increased melting under Pine Island Glacier ice shelf, *Nat. Geosci.*, **4**, 519–523, doi:10.1038/ngeo1188, 2011.

Jenkins, A., Dutrieux, P., Jacobs, S. S., McPhail, S. D., Perrett, J. R., Webb, A. T., and White, D.: Observations beneath Pine Island Glacier in West Antarctica and implications for its retreat, *Nat. Geosci.*, **3**, 468–472, doi:10.1038/ngeo890, 2010.

Konrad, H., Shepherd, A., Gilbert, L., Hogg, A. E., McMillan, M., Muir, A., and Slater, T.: Net retreat of Antarctic glacier grounding lines, *Nat. Geosci.*, **11**, 258–262, doi:10.1038/s41561-018-0082-2, 2018.

Martinson, D. G. and McKee, D. C.: Transport of warm Upper Circumpolar Deep Water onto the western Antarctic Peninsula continental shelf, *J. Geophys. Res.*, **117**, C05012, doi:10.1029/2011JC007618, 2012.

Massonnet, D. and Feigl, K. L.: Radar interferometry and its application to changes in the Earth's surface, *Rev. Geophys.*, **36**, 441–500, doi:10.1029/97RG03139, 1998.

Mazloff, M. R., Heimbach, P., and Wunsch, C.: An eddy-permitting Southern Ocean state estimate, *J. Phys. Oceanogr.*, **40**, 880–899, doi:10.1175/2009JPO4236.1, 2010.

Padman, L., Fricker, H. A., Coleman, R., Howard, S., and Ries, J. C.: A new tide model for the Antarctic ice shelves and seas, *J. Glaciol.*, **64**, 423–439, doi:10.1017/jog.2018.37, 2018.

Rignot, E., Bamber, J. L., van den Broeke, M. R., Davis, C., Li, Y., van de Berg, W. J., and van Meijgaard, E.: Recent Antarctic ice mass loss from radar interferometry and regional climate modeling, *Nat. Geosci.*, **1**, 106–110, doi:10.1038/ngeo102, 2008.

Rignot, E., Mouginot, J., Scheuchl, B., van den Broeke, M., and Kuipers Munneke, P.: Antarctic grounding line mapping from CryoSat-2 radar altimetry data, *Geophys. Res. Lett.*, **38**, L10504, doi:10.1029/2011GL047639, 2011.

Rosen, P. A., Hensley, S., Joughin, I. R., Li, F. K., Madsen, S. N., Rodriguez, E., and Goldstein, R. M.: Synthetic aperture radar interferometry, *Proc. IEEE*, **88**, 333–382, doi:10.1109/5.838084, 2000.

Scambos, T. A., Bohlander, J. A., Shuman, C. A., and Skvarca, P.: Glacier acceleration and thinning after ice shelf collapse in the Larsen B embayment, Antarctica, *Geophys. Res. Lett.*, **31**, L18402, doi:10.1029/2004GL020670, 2004.

Schoof, C.: Ice sheet grounding line dynamics: Steady states, stability, and hysteresis, *J. Geophys. Res.*, **112**, F03S28, doi:10.1029/2006JF000664, 2007.

Seroussi, H., Nakayama, Y., Larour, E., Menemenlis, D., Morlighem, M., Rignot, E., and Khazendar, A.: Continued retreat of Thwaites Glacier, West Antarctica, controlled by weak bed topography and ocean circulation, *Geophys. Res. Lett.*, **44**, 6191–6199, doi:10.1002/2017GL072888, 2017.

Strain, A. J. and Meissner, R.: Tidal height errors around Antarctica, *J. Geophys. Res.*, **109**, C10005, doi:10.1029/2004JC002378, 2004.

Torres, R., Snoeij, P., Geudtner, D., Bibby, D., Davidson, M., Attema, E., et al.: GMES Sentinel-1 mission, *Remote Sens. Environ.*, **120**, 9–24, doi:10.1016/j.rse.2011.05.028, 2012.

Turner, J., Colwell, S. R., Marshall, G. J., Lachlan-Cope, T. A., Carleton, A. M., Jones, P. D., et al.: Antarctic climate change during the 21st century, *J. Geophys. Res.*, **110**, D07103, doi:10.1029/2004JD005462, 2005.

Vaughan, D. G., Marshall, G. J., Connolley, W. M., Parkinson, C., Mulvaney, R., Hodgson, D. A., et al.: Recent rapid regional climate warming on the Antarctic Peninsula, *Clim. Change*, **60**, 243–274, doi:10.1023/A:1026021217991, 2003.

Winton, M., Griffies, S. M., Samuels, B. L., Sarmiento, J. L., and Frölicher, T. L.: Connecting changing ocean circulation with changing climate, *J. Climate*, **26**, 2268–2286, doi:10.1175/JCLI-D-12-00296.1, 2014.

APPENDIX A: HINGE DETECTION ALGORITHM PSEUDOCODE

```
Function DetectHinge(displacement_map, coherence_map):

  // Step 1: Preprocessing
  filtered_displacement = median_filter(displacement_map, kernel=5x5)

  // Step 2: Edge Detection
  grad_x = sobel_x(filtered_displacement)
  grad_y = sobel_y(filtered_displacement)
  grad_magnitude = sqrt(grad_x² + grad_y²)
  grad_normalized = grad_magnitude / percentile(grad_magnitude, 99)
```

```
    // Step 3: Thresholding
    binary_map = (grad_normalized > 0.12) AND (coherence_map >= 0.40)

    // Step 4: Morphological Operations
    opened = binary_opening(binary_map, structure=3x3)
    closed = binary_closing(opened, structure=5x5)
    dilated = binary_dilation(closed, iterations=3)

    // Step 5: Extract Polylines
    hinge_polylines = extract_connected_components(dilated)

    Return hinge_polylines
End Function
```

Study Region: Fimbul Ice Shelf, Antarctic Peninsula
Data Source: ASF Vertex Portal (https://search.asf.alaska.edu/)
Processing Service: ASF HyP3 On-Demand InSAR
Date Prepared: January 2025